Chapter

Tungsten Nanoparticles Produced by Magnetron Sputtering Gas Aggregation: Process Characterization and Particle Properties

Tomy Acsente, Lavinia Gabriela Carpen, Elena Matei, Bogdan Bita, Raluca Negrea, Elodie Bernard, Christian Grisolia and Gheorghe Dinescu

Abstract

Tungsten and tungsten nanoparticles are involved in a series of processes, in nanotechnology, metallurgy, and fusion technology. Apart from chemical methods, nanoparticle synthesis by plasma offers advantages as good control of size, shape, and surface chemistry. The plasma methods are also environmentally friendly. In this chapter, we present aspects related to the magnetron sputtering gas aggregation (MSGA) process applied to synthesis of tungsten nanoparticles, with size in the range of tens to hundreds of nanometers. We present the MSGA process and its peculiarities in the case of tungsten nanoparticle synthesis. The properties of the obtained particles with a focus on the influence of the process parameters over the particle production rate, their size, morphology, and structure are discussed. To the end, we emphasize the utility of such particles for assessing the environmental and biological impacts in case of using tungsten as wall material in thermonuclear fusion reactors.

Keywords: tungsten, nanoparticles, gas aggregation, nanoparticle synthesis, tungsten nanoparticle properties, fusion technology, toxicology of nanoparticles, tritium retention

1. Introduction

1.1 Tungsten nanoparticles: their applications and methods for their synthesis

Tungsten (named also as Wolfram—W) is a material presenting extreme physical and chemical properties, with applications in diverse domains, starting from common life up to high technology. First commercial applications of W started at the beginning of twentieth century when it was used for lighting bulb filaments and in steel alloys. Soon, the domain of applications of W widened, and today it is used

in many fields like lighting, metallurgy, electronics, aviation, medicine, weapons, and so on. An extended description of W properties and applications may be found in literature [1, 2].

Tungsten is also considered to be used as wall material for nuclear fusion reactors, being considered "the best, if not the only, material to withstand the extraordinary operating conditions in a nuclear fusion reactor divertor" [1]. The divertor is situated at the bottom part of the reactor and it is responsible for extraction (during the reactor operation) of the heat and ash produced by the fusion reaction. The heat flux in this region is expected to be in between 10 and 20 MW/m^2 [3] in the International Thermonuclear Experimental Reactor (ITER), leading to local temperatures exceeding 1300°C [4]. Considering the high melting point of W (3422°C), it was selected as material for covering the divertor region in the current design of ITER [5, 6]. Additional properties of W supporting this application of W are: its high thermal conductivity (for removal of heat), low thermal expansion coefficient and low Young modulus (for minimizing the mechanical stresses) and low sputtering yield (for keeping low contamination of the plasma) [1]. Still, the dust generated due to plasma wall interaction may have critical effects on the functioning of the reactor, leading to: (i) cooling of the fusion plasma [7], (ii) accumulation of the fuel in the dust and thus generating possible radioactive safety issues [8] and (iii) biological safety issues regarding dust spreading in case of nuclear accidents such as loss of vacuum accidents [9]. Tests over these effects may be performed using W particles (dust, with dimension starting from nanometric and up to micron range [10, 11]). In addition, tungsten nanoparticles (W NPs) are used in different technological fields, among them being mentioned sintering metallurgy [12], biomedical applications [13] and also microelectronic [14] and spintronic applications [15]. Also, nanoparticles of W oxide (WO_3) have applications including gas sensing [16], photocatalysis (including pollutant degradation [17] and water splitting [18]).

W nanoparticles may be obtained in different ways, which are mentioned bellow. Currently in literature are mentioned various methods for producing W NPs, using different types of chemical and physical processes like: chemical [19] or solvothermal decomposition [20] of W based compounds, mechanical milling [21], vaporization of W precursors in thermal plasma [22], metallic wires explosion [23], laser ablation in liquids [24, 25], growth of W dust in sputtering discharges (i.e. complex plasmas) [26, 27], and by magnetron sputtering combined with gas aggregation (MSGA) [28, 29].

In this chapter, we will focus on the MSGA as method applied for synthesis of W nanoparticles. MSGA method is based on condensation in an inert gas flow of the supersaturated metallic vapors obtained from a magnetron discharge. It was first proposed in 1980's and it was aimed to growth *"strongly adhering thin films formed on room-temperature substrates"* by bombarding the substrate with energetic clusters; the method was first named *"energetic cluster impact"* by the authors [30]. This synthesis method was not found feasible for industrial thin films deposition, due to low efficiency of the process [31, 32]. Despite of this, it is applied to the moment by many research groups for synthesis of metallic nanoparticles (Ag, Cu, Fe, Cr, Ti, etc.) [33, 34], polymers [35] or even more complex types of structures (like bimetallic [36] or core-shell [37] nanoparticles) because, compared with other synthesis methods, MSGA has several advantages. Thus, the cluster sources based on MSGA are compatible with vacuum processes, are used in numerous technologies [38], are well controlled, and the obtained samples present a high chemical purity.

W NPs obtained by MSGA were reported for the first time by us in [28]. Further works were related to studies regarding tritium absorption and retention [39, 40] in this material and W NP cytotoxicity [41–43]. These experiments will be also presented briefly in this chapter.

1.2 Structure of the chapter

After the short Introduction presented above, the chapter continues with a short section mentioning the basic aspects of the process. Then, a typical system used for synthesis of nanoparticles, particularized in the case of Tungsten is discussed. We point out on the experimental system geometry and on the most important experimental parameters. These include the chemical nature of the working gas, the values of the electrical power applied to the discharge, and the thickness of the target. We present two characteristics, important for any material synthesis process: the deposition rate and the dimension of the deposit on the substrate. Thus, we point out on the decrease (down to near zero) of the synthesis rate in time (tens of minutes) if only Ar is used as working gas. The method for increasing and stabilizing the synthesis rate is also presented.

One of the sections is devoted to the properties of synthesized materials, respectively of the W NPs (including their morphology, size, and structure), obtained at various working parameters. Herewith, the effect of residual gases, and H_2 addition in the discharge over the nanoparticles morphology are emphasized.

Finally, we briefly describe some applications of the W NPs, namely those related to fusion technology and to cytotoxicity evaluation.

2. Formation of particles during magnetron sputtering and gas aggregation

In the field of material physics, clusters are defined as small, multi-atoms objects; if their dimension is in between 0 and 100 nm, they are named as nanoparticles. One of the physical methods for atomic clusters (or nanoparticles) synthesis is gas aggregation. This is a bottom-up method and consists in condensation of a supersaturated vapor (obtained from the material of interest) in a flow of cold inert gas. The supersaturated vapor atmosphere is obtained by different methods, including: thermal evaporation, laser ablation, magnetron plasma sputtering, etc. All these techniques are feasible to be implemented for metals with relative low melting and evaporation points [32]. It is obviously that for W, possessing the highest melting (3422°C) and evaporation points (5930°C) from all metals, only laser ablation and magnetron plasma sputtering are feasible to be implemented. This work presents the results obtained using a magnetron sputtering based cluster source.

By sputtering, atoms are obtained from a solid target due to its bombardment with ions produced in plasma; the presence of the magnetic field crossed with the electrical one (typical for magnetron sputtering devices) leads to a high rate of atoms production; more details regarding magnetron sputtering technique may be found elsewhere [44, 45].

Formation of clusters/nanoparticles is described detailed in different textbooks [32, 46]; for the sake of clarity, we will present this process briefly here. Thus, synthesis of clusters can be considered to take place in two successive steps: nucleation and growth. Nucleation may be defined as the process by which embryos of a stable phase are formed in a surrounding thermodynamically metastable phase [46, 47]. In MSGA source, the metastable phase consists of a supersaturated vapor of metal particles, which is obtained due to the decrease of the temperature of the sputtered atoms when they depart from the target. Interaction between the supersaturated vapor of metal (Me) with the colder buffer gas (Ar) leads to nucleation of metal particles, this process being described in the term of a three-body process Eq. (1):

$$Me + Me + Ar \rightarrow Me - Me + Ar \quad (1)$$

where the inert gas atom (Ar) takes the excess of energy resulting from the Me–Me dimer formation; the dimers Me–Me are the embryos for the further growth of the nanoparticles. In MSGA process, the nucleation is usually homogeneous, appearing spontaneously and randomly, without preferential sites of nucleation. In contrast, in some situations, the Me–Me dimers are not stable in plasma and the nucleation is dependent on the presence of an external factor, like a reactive gas in a well-defined amount. For example, this situation is encountered during synthesis of Ti or Co nanoparticles by MSGA. Apparition of the nucleation sites is conditioned in this situation by the presence of small amounts of reactive gases (O_2, respective N_2) mixed with Ar [48]. Also, we observed that nucleation of W nanoparticles is dependent on the presence of H_2 mixed with Ar in the cluster source. In contrast, nucleation of Cu nanoparticles in MSGA is not dependent on the presence of any reactive gases, their nucleation appearing in sole Ar, and being practically not influenced by the presence of O_2 in discharge [49].

Briefly, the steps of nanoparticles formation and growth are the following ones [46, 47]. After the formation of the initial embryos, further growth takes place by four main processes: *attachment* of the atoms (or *condensation*), coagulation, coalescence and aggregation. During the first process, the number of the atoms from a cluster increases due to *attachment* of supplementary metal atoms; the supplementary energy gained due to bonds formation is dissipated during the collisions between the growing clusters with the buffer gas atoms. The second type of processes (*coagulation*) happens when two clusters (each containing n and respective m atoms) are unified, forming a larger cluster (containing $n + m$ atoms). This process is similar to the formation of a liquid drop following the contact of two smaller liquid drops. The third type of processes (*coalescence*), takes place when the supersaturation degree is low and it consist in growth of larger clusters by atom attachment, while the smallest ones evaporate. Finally, during *aggregation*, two clusters come in contact without modification of each one shape, forming a larger cluster.

3. Experimental

3.1 Experimental setup

A typical magnetron sputtering gas aggregation (MSGA) system for production of nanoparticles is presented schematically in **Figure 1**. It consists of a cluster source

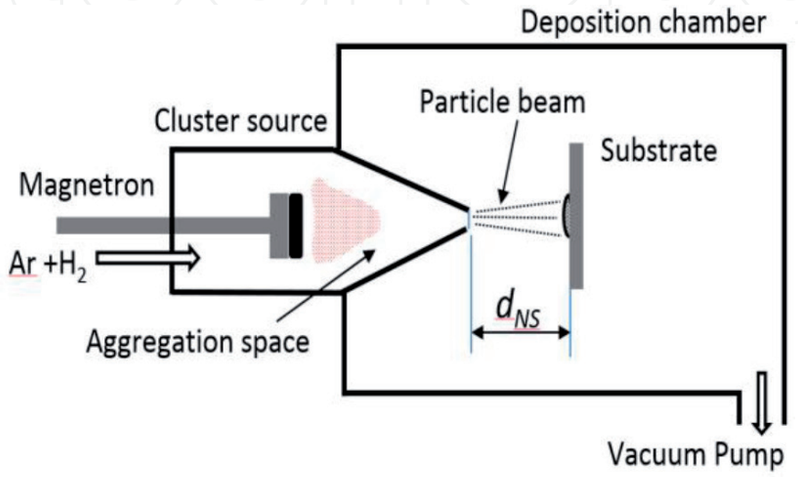

Figure 1.
Schematic of the MSGA experimental system used for nanoparticles synthesis.

ending with an aperture, attached to a high vacuum chamber similar with those used for thin film deposition. The enclosure of the cluster source is a cylindrical stainless steel tube with water cooled walls; a magnetron sputtering gun is mounted axially in it, with the target facing the exit aperture. The nanoparticles synthesis takes place in the space between them (see **Figure 1**). The working gas (an inert gas used in sputtering, usually Ar) enters in the system through the cluster source and it is evacuated by a vacuum pumping system attached to the deposition chamber.

Due to its small diameter (typically a few millimeters), the exit aperture presents a small gas flow conductance, resulting in development of a differential pressure between the cluster source and the deposition chamber. As a consequence, the nanoparticles obtained in the aggregation space of the cluster source are ejected in the deposition chamber, where they are collected on the substrate.

The properties of the nanoparticles obtained by MSGA depend on the process parameters (pressure, applied power, working gas type, etc.) and on the geometrical characteristics of the cluster source (including the distance between the target and the nozzle, and the nozzle diameter) [32]. In the present study, we considered a part of these parameters, and we report on the effects of changing the RF power, target thickness and nature of admixed gases.

3.2 Materials and characterization methods

The nanoparticles presented herein were obtained from circular W targets with 99.95% purity. Their diameter is of 2 inches while two thicknesses were used (6 and 3 mm).

The low-pressure Torus TM2 (Kurt Lesker Co.) was adapted in laboratory for use in the high pressure range (tens of Pa). The plasma discharge was sustained by a RF (13.56 MHz) power generator (model Comet CITO PLUS 1000 W) paired with a corresponding matching box (model Comet AGS 1000 W). The RF generator was operated either in continuous wave mode or in pulsed mode.

The process gas was Ar or a mixture of Ar with different other gases (H_2, O_2, water vapors), the pressure of the working gas being of 80 Pa in cluster source (0.5 Pa in the deposition chamber).

The exit aperture of the MSGA cluster source was 2.5 mm while the aggregation length was 5 cm for all studies presented here. The generated nanoparticles were collected on two types of substrates: monocrystalline Si substrates chips and microscope slides.

The deposited nanoparticles were investigated as regarding their material properties as follows.

The morphology was investigated by scanning electron microscopy (SEM), using an EVO 50XVP Zeiss device equipped with LaB6 electron gun operating at 20 kV. The nanoparticles microstructure was analyzed by high resolution transmission electron microscopy (HRTEM), using a Cs probe-corrected atomic resolution analytical electron microscope JEOL JEM-ARM 200F, operated at 200 kV.

The crystalline structure of the deposited samples was investigated by X-ray diffraction (XRD) using a PANalytical X'Pert PRO MRD diffractometer (wavelength CuK-α 0.15418 nm) equipped with a point sensitive fast detector (PIXcel) operated in Bragg–Brentano geometry.

3.3 Deposition rate: shape of the deposit on the substrate

The experiments of W NPs synthesis by MSGA were reported for first time by us [28, 29] using as working gas sole Ar. These were performed using RF power in both continuous wave (60 W [28] and 100 W [29]) and in rectangular pulsed mode [29]

(RF power was switched ON/OFF at intervals of 200 ms, duty cycle 50%, the maximum RF power being 120 W and the minimum one being zero, i.e. an average value of 60 W). The other experimental parameters were kept constant.

The deposition rate was evaluated by weighting the substrates before and after deposition. Despite of different values of electrical power applied to the discharge, we observed similar deposition rates, around 5 mg/h. On the other hand, we observed a gradual decrease of the deposition rate in time.

Figure 2a presents the image of a substrate (microscope slide), which was periodically translated vertically in front of the exit aperture, after 5 min deposition. The substrate was positioned at d_{NS} = 2.5 cm distance from the exit aperture. We can observe the decrease of the spot diameters, from around 1 cm at the process beginning (see the lower spot, at t = 0, in **Figure 2a**) down to few millimeters after 20 min (see the upper spot in the same figure). This fact proves that the deposition rate decreased down to near zero after a finite time duration. Still, after breaking the vacuum and exposing the target for few hours to the ambient atmosphere the W NPs process takes place again. A similar decrease of the deposition rate was reported in [48] during synthesis of Ti and Co nanoparticles using the MSGA technique. For these materials, it was proved that the generation of nucleation sites is conditioned by the presence of small amounts of reactive gases (O_2 for Ti, respective N_2 for Co) mixed with Ar in the aggregation chamber. Similarly, we identified by trials that mixing Ar (5 sccm) with a small amount of H_2 (0.7 sccm) revitalizes the synthesis process, leading to continuously deposition of W NPs at an average rate of 50 mg/h.

The nanoparticles are ejected from the cluster source as a conical beam, resulting that the diameter of the deposit formed on the substrate is dependent on the substrate position in respect to the exit aperture of the cluster source. For example, placing the substrate at a distance of 27 cm in respect to the nozzle, the deposited material extends over a spot area of 5 cm spot diameter (see **Figure 2b**) in case of using a mixture Ar/H_2. Thus, modifying the substrate position in the deposition chamber, the diameter of the deposited spot may be modified from 1 cm up to 5 cm, as it is described by **Figure 2c**. This aspect is important for applications where particles distributed over large areas are in demand.

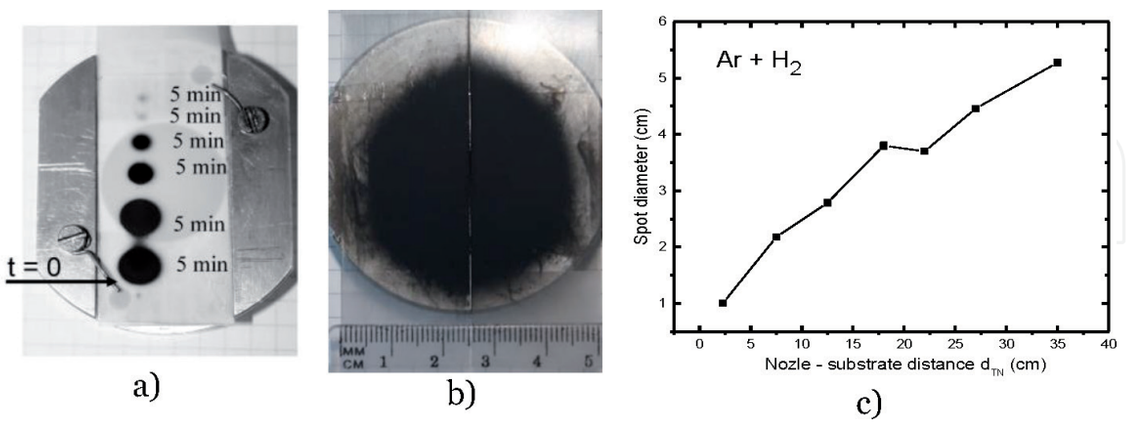

Figure 2.
(a) Time evolution of the W NPs deposit when only Ar is used as working gas; (b) example of a deposition performed in mixture Ar + H_2, the substrate being placed at a distance of 27 cm from the nozzle; (c) dimension of the W NP deposits over the position of the substrate (using Ar + H_2 mixture).

3.4 Morphology and structure of the nanoparticles: effect of the RF power applied to discharge on the particles properties

The results presented in this section were obtained using only Ar as working gas, at a mass flow rate of 5 sccm; the corresponding pressures in the aggregation and

deposition chambers being 80 Pa, respective 0.5 Pa. A 6 mm thick target was used, the tangential magnetic field at the target surface being of 100 mT.

Plasma was generated either in continuous, either in pulsed power mode, as follows:

- continuous wave operation mode, applying 60 W and 80 W RF power to the discharge;

- pulsed wave operation mode, with a medium power of 60 W (P_{max} = 120 W, P_{min} = 0 W, the pulsing durations being t_{ON} = t_{OFF} = 200 ms).

No significant modification of the W NPs synthesis rate was observed when the RF power value was increased (in continuous mode) or was pulsed. Instead of this, the obtained nanoparticles present totally different material properties.

SEM images of the deposited nanoparticles are presented in **Figure 3a** (P_{RF} = 60 W), **Figure 4a** (P_{RF} = 100 W) and **Figure 5a** (pulsed mode). At first glance, it is obviously that the morphology of the nanoparticles is dependent on the power applied to the discharge. Thus, on the sample deposited at 60 W (**Figure 3a**) can be observed both individual nanoparticles (of around 70 nm in diameter) and agglomerations of such nanoparticles. These agglomerations are most probably to appear inside the aggregation chamber, being promoted by electrostatic attraction of the nanoparticles [50]. Increasing the applied RF power up to 100 W the nanoparticles shape changes to concave hexapods (**Figure 4a**), with dimension in between 80 and 200 nm. In pulsed mode, the nanoparticles are round and on the sample can be observed (**Figure 5a**) two classes of nanoparticles: faceted ones, with dimension between 40 and 80 nm (higher number) and flower like ones with dimension in between 80 and 100 nm (smaller number).

The nanoparticle shapes are highlighted by the low magnification TEM images presented in **Figure 6a** (P_{RF} = 60 W), **Figure 7a** (P_{RF} = 100 W) and **Figure 8a** (pulsed mode). Supplementary, TEM images reveal that nanoparticles deposited in continuous wave mode present a dendritic growth, their branches evolving in flower like (**Figure 6a**, P_{RF} = 60 W) or star like pattern (**Figure 7a**, P_{RF} = 100 W). TEM images of faceted nanoparticles obtained in pulsed mode present projections containing 8 or 6 sides, suggesting a cube-octahedral geometry for these nanoparticles (see the inset image in **Figure 8a**) [51].

The XRD patterns recorded on the deposited samples are presented in **Figure 3b** (P_{RF} = 60 W), **Figure 4b** (P_{RF} = 100 W) and **Figure 5b** (pulsed mode). The peaks from these diffraction patterns show the presence in the sample of the

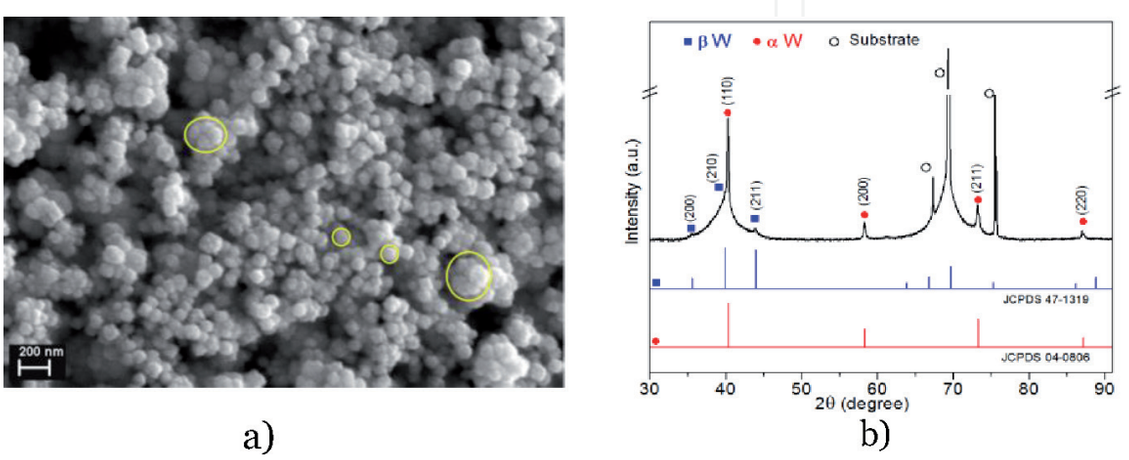

Figure 3.
SEM image (a) and the XRD pattern (b) of the W NPs deposited at 60 W applied to discharge.

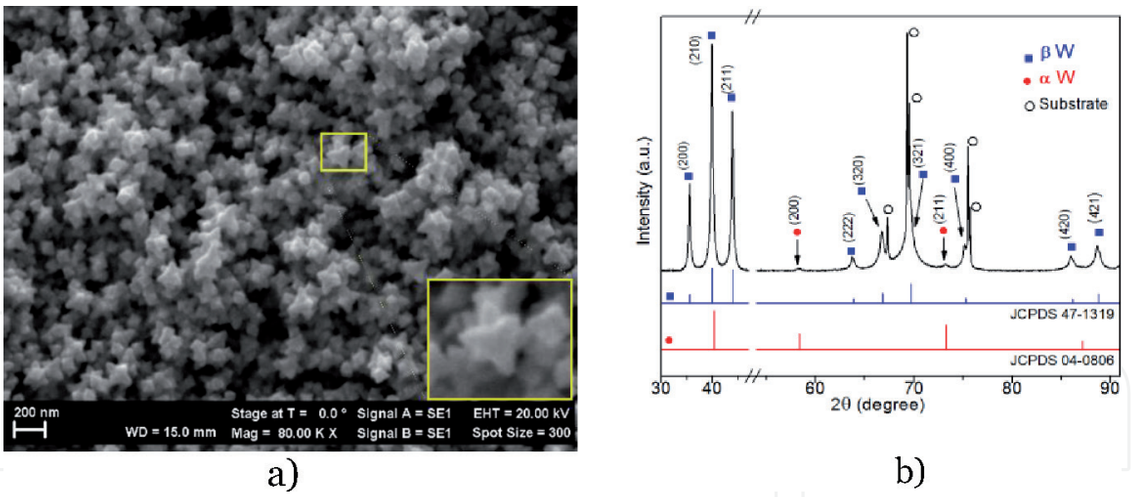

Figure 4.
SEM image (a) and the XRD pattern (b) of the W NPs deposited at 100 W applied to discharge.

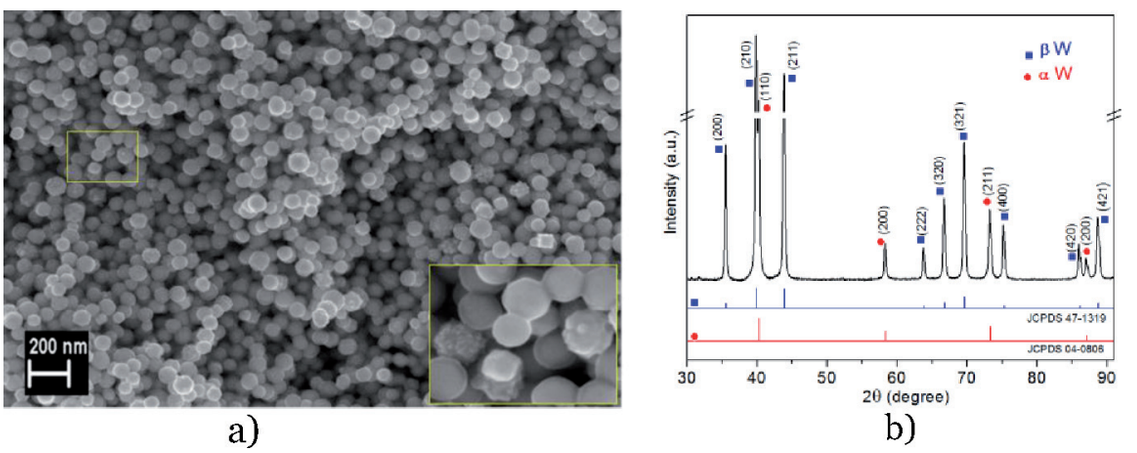

Figure 5.
SEM image (a) and the XRD pattern (b) of the W NPs deposited using pulsed RF power.

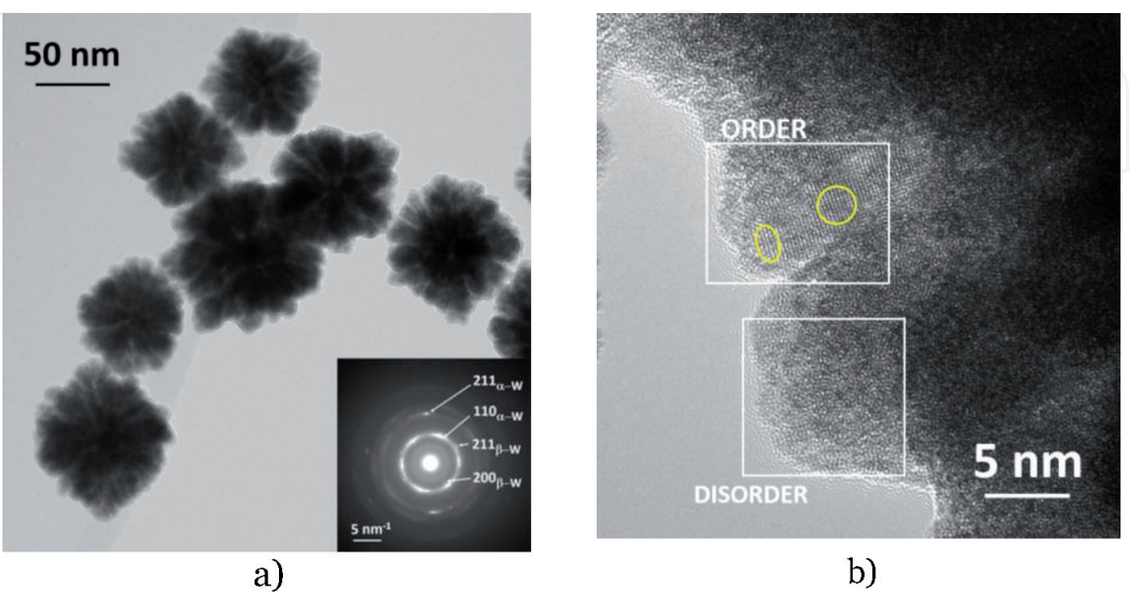

Figure 6.
TEM (a) and HRTEM (b) images recorded on W NPs deposited at 60 W applied to discharge.

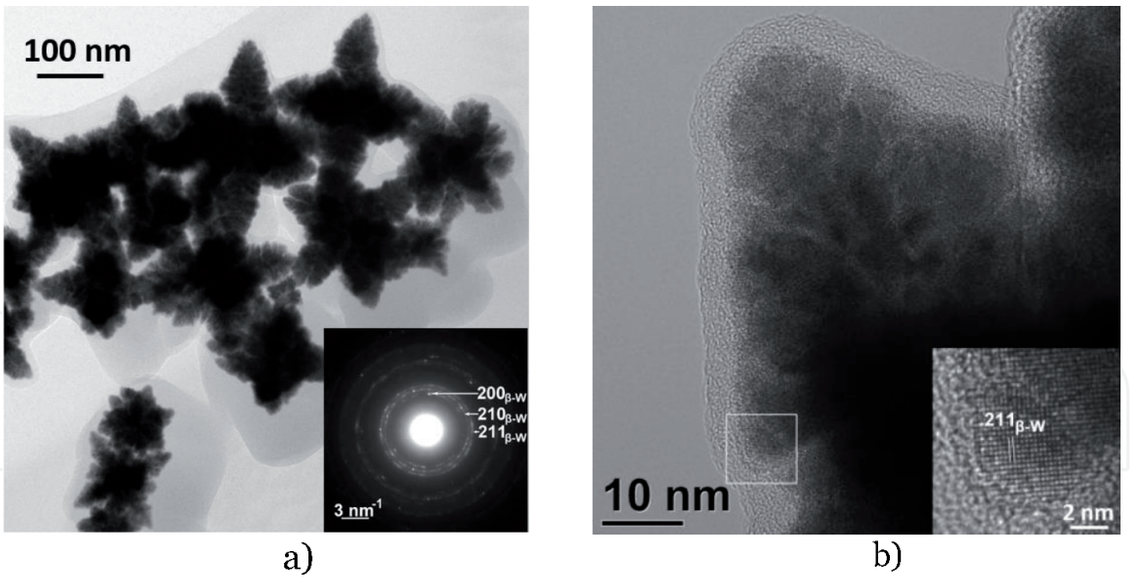

Figure 7.
TEM (a) and HRTEM (b) images recorded on W NPs deposited at 100 W applied to discharge.

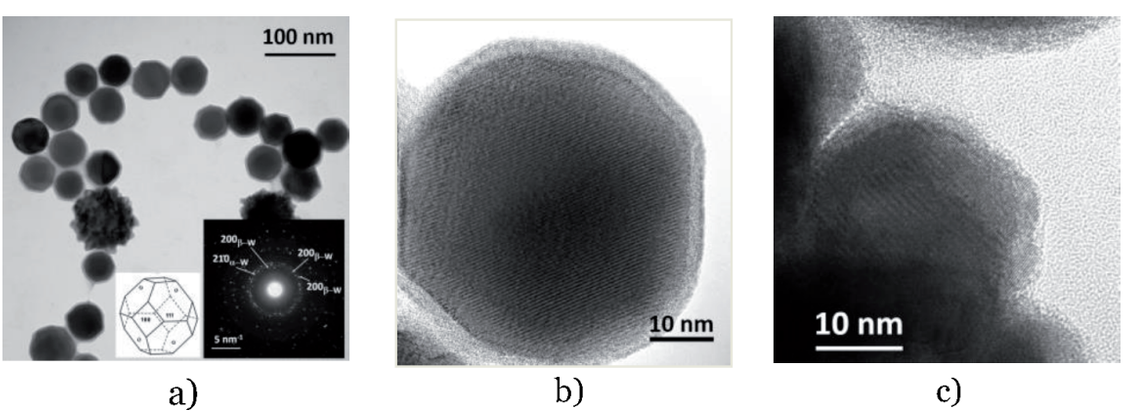

Figure 8.
TEM (a) and HRTEM images recorded on cuboctahedral W NPs (b) and on a flower like one (c), deposited using pulsed RF power.

body-centered cubic lattice (bcc) α-W (JCPDS 04-0806) and of the simple cubic A15 lattice, corresponding to metastable β-W phase (JCPDS 47-1319). It is interesting to note that the α-W phase is dominant in nanoflower samples (**Figure 3b**) while the β-W one in the nano hexapod samples (**Figure 4b**); on the other hand, the samples deposited with pulsed RF power present similar contributions from the both α-W and β-W phases. A remarkable result is the observation that the β-W (which is usually metastable, converting rapidly to α-W even at room temperature) remained unchanged even after 2 years of storage in laboratory environment (more details can be found in [28]).

The HRTEM images recorded on the samples reveal that in the branches of the nanoflowers (**Figure 6b**) coexist regions with high order or with high disorder. This observation is confirmed also by the shape of the XRD peaks (with sharp peaks and enlarged bases, (see **Figure 3b**) and by the appearance of the SAED pattern recorded (presence of both bright spots and broad diffraction rings in the diffraction pattern; see inset in **Figure 6a**). On the other hand, the hexapods and cube octahedral present a much higher degree of crystalline order in the samples.

Indeed, the HRTEM image from **Figure 7b** shows well textured regions, in the inset of the figure being presented well-defined nanocrystallites with size of around

5–6 nm, that form each branch. On the other hand, the cube octahedral nanoparticles are single nanocrystals (see **Figure 8b**). Also, the branches of the nanoflowers incidental observed in **Figure 8a** show a higher degree of order (see **Figure 8c**) when compared with those grown at 60 W (see **Figure 6b**). These observations are supported also by the SAED patterns presented as insets in **Figures 7a** and **8a**, both presenting only bright spots. Details regarding the chemical composition of the W NPs and their oxidation in ambient air can be found elsewhere [28, 52]. We briefly mention here that the amorphous layers which can be observed on the edges of the nanoparticles (see HRTEM images from **Figures 7b** and **8b**) are due to post synthesis oxidation.

3.5 The effect of target thickness on the morphology of W NPs

We already mentioned that we used W targets with thicknesses of 3 mm, respective 6 mm. In fact, modifying the thickness of the targets we took into account the effect of the magnetron magnetic field over the nanoparticles synthesis process. Thus, for 6 mm targets the measured value of the tangential magnetic field at the target surface was 100 mT, while it was 150 mT for 3 mm targets. In this section we present the morphologies of the W NPs obtained with a 3 mm thick target, following a parametric study involving the variation of the RF power applied to the discharge. The working gas is Ar only. During the study the other experimental parameters were kept constant (identical with those used in the previous section): aggregation length of 5 cm, nozzle diameter of 2.5 mm, the substrate being situated at 2.5 cm from the nozzle. Thus, similar with previous experiments, the Ar mass flow rate was kept at a value of 5 sccm, while the value RF power applied to the discharge (in continuous wave mode) was varied in between 60 and 120 W, with steps of 10 W.

All the samples were deposited on Si substrates and these were further investigated by SEM. These investigations show that in general the deposited samples contain particles with different morphologies on the same substrate. Only two samples (for the applied powers of 60 and 80 W respectively) were observed to contain particles with the same morphology; the SEM images recorded on these samples are presented in **Figure 9**.

For 60 W RF power the nanoparticles present a nanoflower like morphology, similar with those obtained in the same conditions with a thick target (see **Figure 3a**). Their dimension is also similar, being in between 50 and 100 nm. Still, we have to note that the sample of W NPs obtained with a thinner target presents a much lower degree of agglomeration (compare **Figure 3a** with **Figure 9a**).

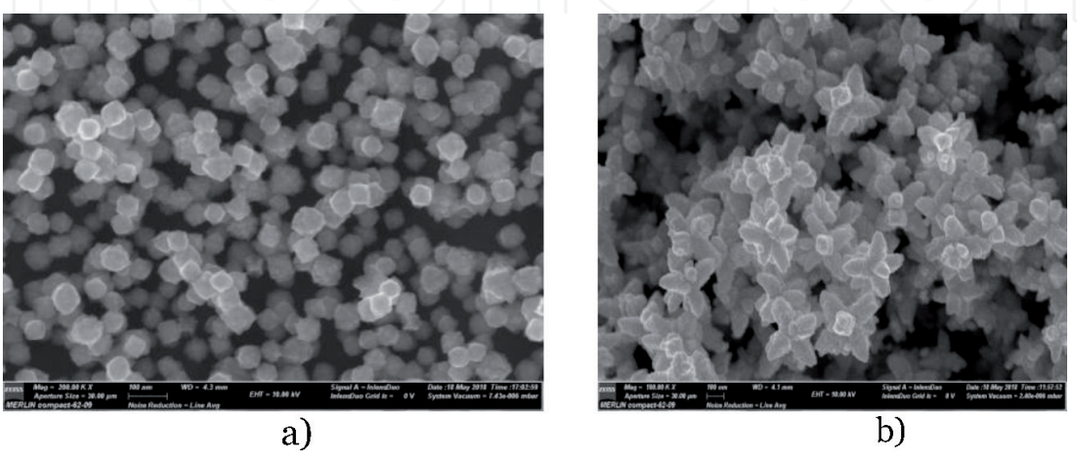

Figure 9.
SEM images recorded on substrates deposited at: (a) 60 W (nanoflowers) and (b) 80 W (multiple branches); Scale bar 100 nm.

For 80 W RF power applied to discharge, the obtained particles are in fact multipodal nanostructures, with up to 8 emerging branches. The distance between the tips of two opposite branches ranges in between 350 and 400 nm, while the diameter of one branch measure around 80–90 nm. These structures seem to be similar with hexapod nanoparticles obtained with thick W target (see **Figure 4**).

For the remaining samples deposited with different values of the RF power, the samples are not uniform in respect with the particles morphology. Examples of SEM images recorded on two of such samples (at 70 and 110 W) are presented in **Figure 10**. Here we can observe flower like, faceted, with sharp corners, and even cubic nanoparticles.

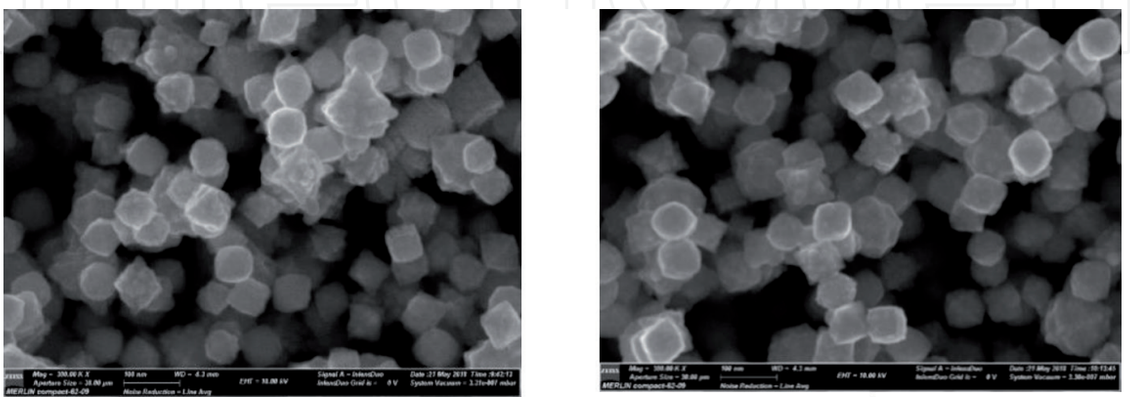

Figure 10.
SEM images recorded on substrates deposited at 70 W (a) and 120 W (b); each sample contains particles with different morphologies. Scale bar 100 nm.

3.6 The effect of residual gases in discharge on the W NPs morphology and synthesis rate

As mentioned, the decrease of deposition rate down to zero in short time after the beginning of the MSGA process leads us to the hypothesis that nucleation of W NPs in MSGA may be assisted by the residual gases present in the aggregation chamber. For testing this hypothesis, we inserted deliberately small amounts of gases from the atmospheric air components in the discharge, immediately after the deposition ceasing for the process performed in Ar. We observed that mixing H_2 or water vapors with Ar in the aggregation source leads to the revitalization of the MSGA synthesis process, leading to a continuous synthesis of W NPs, at higher deposition rate; it seems that O_2 does not have such effect over the deposition rate. However, a side effect of mixing of other gases with Ar in the aggregation chamber is the modification of the nanoparticles morphologies.

We note that these experiments were performed in continuous wave, with a 6 mm thick W target. **Figure 11** presents SEM images recorded with different gases added in the discharge.

By comparing **Figure 11a** with **Figure 3a** it results that addition of H_2O vapors in the discharge at an applied power of 60 W leads to less agglomerated particles. Apart from nanoflower morphology, also appear particles with sharp corners, while the dimension of particles increases (from up to 50–100 nm in dry Ar, up to 100–250 nm in humid Ar). Like we already mentioned, the synthesis rate increases significantly.

Addition of O_2 in the discharge does not increase the synthesis rate, but modifies significantly the particles shape. This can be observed by comparing **Figure 11b** (round nanoparticles) with **Figure 4a** (hexapod nanoparticles). These samples

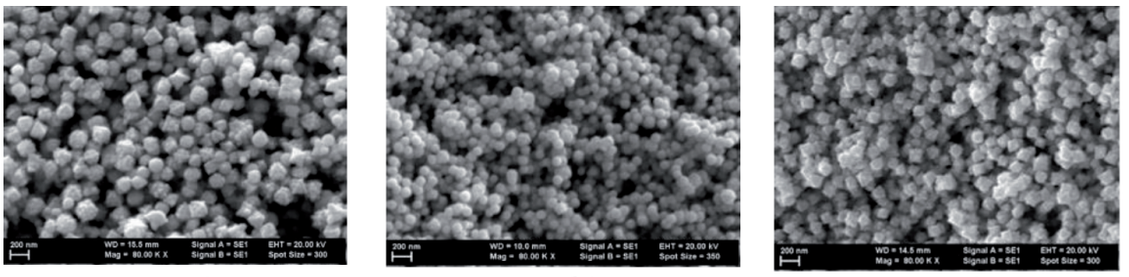

Figure 11.
SEM images recorded on substrates deposited with W NPs in Ar (5 sccm) mixed with different other gases: (a) H_2O vapors (0.5%), at 60 W; (b) O_2 (0.03 sccm) at 100 W and (c) O_2 (0.03 sccm) + H_2 (0.1 sccm) at 100 W.

were deposited in similar conditions, at 100 W RF, the single difference being addition of a very small amount of O_2 (0.03 sccm) in the main process gas (Ar, 5 sccm). Enriching this Ar/O_2 mixture with H_2 (0.1 sccm) leads to further change in morphology, from round nanoparticles (**Figure 11b**) to particles presenting corners (**Figure 11c**). H_2 seems to favor anisotropic growth (particles with sharp corners), while O_2 seems to favor isotropic growth (round NPs). Therefore, addition of H_2 sustains the synthesis of W NPs and leads to the increase of deposition rate.

4. Use of tungsten nanoparticles for toxicology studies and assessment of tritium retention in nuclear fusion technology

Expected power and plasma duration of future fusion devices, such as ITER, requires the divertor plasma-facing components (PFC) to withstand considerable plasma fluxes (up to 10 MW/m^2 and 10^{23} H m^{-2} s^{-1}). In this area, tungsten has been chosen for its good resistance to high temperature and its low plasma sputtering yield. However, experiments have shown that the combination of different phenomena (e.g. melting of edges of PFC, material fatigue, intense particle fluxes, material erosion followed by accretion in the plasma edge, ...), particularly during off normal events such as Edge Localized Modes (ELMs) or disruptions, can trigger the formation of particles. They will experience variable size, from tens of nanometers to hundreds of micrometers. Compared to the current tokamaks, the expected energy outflows are much higher in ITER. Larger quantities of dust will be produced. Besides, impurities in the Scrape-Off Layer (SOL), such as oxygen, metals and especially gas radiators are expected to enhance physical sputtering of the PFC materials. Generated particles will be hence tritiated as formed in a tritium environment.

Safety limits have been set for the inventory of tritium in the vessel (for which dust particles can contribute), but also for the quantity of dust to avoid explosive hazards. Even if dust production in present tokamaks is less important, it is of a major importance, in order to prepare a safe ITER operation, to investigate how relevant dust can store tritium. Indeed, such tritiated particles could be released in case of a Loss Of Vacuum Accident (LOVA) and be accidentally inhaled by ITER workers. Harmful consequences will depend on the dust physicochemical characteristics and the inhaled dose. It is the reason why we have decided to investigate their potential biological toxicity. To this end, several actions are to be undertaken: understanding and characterizing the interaction of particles with tritium and studying the biological impact of these tritiated dusts on human lung cells.

As said above, the current dust tokamak production is scarce and dust relevant particles have to be produced. Different production methods have been approached, among them being MSGA, milling, and laser ablation. The properties of the

nanoparticles produced by magnetron sputtering gas aggregation are of major interest. Indeed, such particles size have the size ranging from 100 to 200 nm, therefore present the maximum probability to escape the High Efficiency Particulate Air (HEPA) filters, normally used to prevent as much as possible the release of particles out of the vacuum chamber.

4.1 Tritium retention in tungsten dust

To study this topic, after particle production, tritiation has been undertaken using the usual gas loading procedure with tritium followed at the Saclay tritium laboratory [53]. The procedure involved various steps, like native oxide layer removed by reduction under hydrogen atmosphere, loading of tritium, cooling the sample at liquid nitrogen temperature to freeze the tritium detrapping processes, thus leading to tritium saturation in particles. For comparison during toxicity studies, particles are also hydrogenated in the same way than for the tritium loading. Particle tritium inventory is obtained by desorption and by full dissolution of the samples in water peroxide and liquid scintillation counting. In case of MSGA type of particle, it is about 5 Gbq/g. These values are two or three orders of magnitude higher than in massive samples, where 11.5 MBq/g were measured [39].

4.2 Cytotoxicity of tungsten nanoparticles

The study of consequences of inhaling small W particles that can reach the human inner lung or can come in contact with the skin, as first organ barriers, is of high importance. Different topics are thus addressed such as the behavior of particles and embedded tritium in biologic media or the in vitro toxicity of these tritiated particles [54]. It is worth to note that the particles are rapidly dissolved (less than 1 week) in different biologic media as saline solution, TRIS buffer, and cell culture medium lung solution. TRIS solution is usually used to prepare particle stock solution for in vitro studies. The consequence of the dissolution of the particles is the release of tritium into the solution. Tritium, once solubilized, will be removed quickly as it has been shown that tritium in tritiated water form is eliminated very quickly from the human body (half-life of 10 days).

The toxicity of W particles produced by milling was evaluated on the MucilAir® model [55], a 3D in vitro cell model of the human airway epithelium grown on air-liquid-interface [42]. Epithelia were exposed to tungsten nanoparticles (tritiated or not) for 24 h. Thanks to the long shelf life of this model, cytotoxicity was studied immediately after treatment and in a kinetic mode up to 1 month after cell exposure to assess the reversibility of toxic effects. Acute and long-term toxicities were monitored by several endpoints: (1) epithelial integrity, (2) cellular metabolic activity, (3) pro-inflammatory response, (4) mucociliary clearance, and (5) morphological modifications. Transmission Electronic Microscopy (TEM) observations, inductively coupled plasma mass spectrometry (ICP-MS) measurements and liquid scintillation were performed to determine tungsten and tritium lung absorption as well as intracellular accumulation. On this human lung epithelium model, no significant toxicity was observed after exposure to ITER-LIKE particles produced by milling followed by 28-day kinetic analysis. Moreover, tritium transfer through the epithelial barrier was found to be limited in comparison with the complete transfer of tritium from tritiated water. These data provide preliminary information to biokinetic studies aimed at defining biokinetic lung models to establish new safety rules and radiation protection approaches.

In respect with usage of MSGA and laser ablation particles in toxicology studies, the behavior of cells from bronchial human-derived BEAS-2B cell line with such

particles in their pristine, hydrogenated, and tritiated forms is described in [43]. Cell viability, cytostasis and DNA damage were evaluated by specific biological assays. The study concludes that long exposures (24 h) induced significant cytotoxicity, the effect being enhanced in case of the hydrogenated particles. Epigenotoxic alterations were observed for both MSGA and laser ablation types of particles. Due to the observed oxidative dissolution of W nanoparticles in liquid media, such effects might be related to the presence of W^{6+} species in the medium.

The toxicity of MSGA tungsten nanoparticles on human skin fibroblast cells (BJ ATCC CRL 2522), was evaluated in [56]. Different concentrations of tungsten nanoparticles (1–2000 μg/mL) added in liquid medium were used. MTS colorimetric tests and Scanning Electron Microscopy in secondary electrons (SE) and backscattering (BSE) operating modes were used to observe the effects. At low concentrations of nanoparticles in suspension, no toxic effects were observed by the MTS colorimetric test. However, when the nanoparticle concentration added to the cellular medium increases above 100 μg/mL, reaching even 1 mg/mL and 2 mg/mL, the toxicity of tungsten nanoparticles is high. The cell morphology changed, in comparison with the control sample. Cells tend to become round, a sign that precedes their death. At a higher magnification, in BSE mode, it is noticeable that the nanoparticles may be internalized under the cell membrane.

5. Conclusions

This chapter describes a physical method of fabrication of nanoparticles, namely Magnetron Sputtering Gas Aggregation (MSGA). The advantages come from a clean plasma-based process which do not make use of wet chemistry, and is well controlled, and reproducible. The synthesis of tungsten particles was selected to illustrate the potential of the method. Not only those particles are promising materials for nanotechnological devices, photocatalysis, and energy storage, but environmental and toxicological questions raised by the occurrence of tungsten dust in fusion experiments request answer of high importance for the scientific community working in the fusion energy research. The produced particles, analyzed in this chapter, have size in the range 100–200 nm, and have, depending of the applied plasma power, flower like, hexapod, or cube-octahedral morphologies. Mixture of these morphologies in the same sample is also possible at other parameters. The particles are single crystals in case of cube-octahedral morphology (pulsed applied power), or consists of small nanocrystallites (3–5 nm) which are assembled in a disordered manner (in nanoflowers, at P_{RF} = 60 W), or in a much-ordered manner (in nanohexapods, at P_{RF} = 100 W). The W dust consisting of such particles incorporates tritium amounts of two to three orders of magnitude higher than the massive tungsten material. Although limited in respect with the conditions of exposure and types of cells, the biological studies mentioned in the chapter indicate that the toxic effects should be considered in the activities involving W dust, especially at large concentrations of particles.

Acknowledgements

Part of this work has been carried out within the framework of the Eurofusion consortium and has received funding from the Euratom research and training program 2014–2018 and 2019–2020 under grant agreement no. 633053. The views and opinions expressed herein do not necessarily reflect those of the European Commission. In addition, we acknowledge the support in the frame of

the Romanian PN-III-P1-1.2-PCCDI-2017-0637/33 PCCDI (MultiMonD2) and INFLPR Nucleus projects, and the support of the A*MIDEX project (no. ANR-11-IDEX-0001-02) funded by the "Investissements d'Avenir" French Government program, managed by the French Research Agency (ANR).

Conflict of interest

The authors declare that there is no conflict of interest.

Author details

Tomy Acsente[1], Lavinia Gabriela Carpen[1,2], Elena Matei[3], Bogdan Bita[1,2], Raluca Negrea[3], Elodie Bernard[4], Christian Grisolia[4] and Gheorghe Dinescu[1,2*]

1 National Institute for Lasers, Plasma and Radiation Physics, Bucharest, Romania

2 Faculty of Physics, University of Bucharest, Bucharest, Romania

3 National Institute of Materials Physics, Bucharest, Romania

4 CEA, IRFM, Saint Paul lez Durance, France

*Address all correspondence to: dinescug@infim.ro

References

[1] Lassner E, Schubert W-D. Tungsten, Properties, Chemistry, Technology of the Element, Alloys, and Chemical Compounds. USA: Springer; 1999. p. 447. DOI: 10.1007/978-1-4615-4907-9

[2] 20 Interesting Facts About Tungsten [Internet]. 2019. Available from: https://briandcolwell.com/20-interesting-factsabout-tungsten/ [Accessed: 31 January 2020]

[3] ITER [Internet]. Available from: https://www.iter.org/mach/Divertor [Accessed: 31 January 2020]

[4] Gunn JP et al. Surface heat loads on the ITER divertor vertical targets. Nuclear Fusion. 2017;**57**(4):046025. DOI: 10.1088/1741-4326/aa5e2a

[5] Pitts RA, Carpentier S, Escourbiac F, Hirai T, Komarov V, Lisgo S, et al. A full tungsten divertor for ITER: Physics issues and design status. Journal of Nuclear Materials. 2013;**438**:S48-S56. DOI: 10.1016/j.jnucmat.2013.01.008

[6] Philipps V. Tungsten as material for plasma-facing components in fusion devices. Journal of Nuclear Materials. 2011;**415**:S2-S9. DOI: 10.1016/j.jnucmat.2011.01.110

[7] Winter J, Gebauer G. Dust in magnetic confinement fusion devices and its impact on plasma operation. Journal of Nuclear Materials. 1999;**266-269**:228-233. DOI: 10.1016/S0022-3115(98)00526-1

[8] Rosanvallon S, Grisolia C, Delaporte P, Worms J, Onofri F, Hong SH, et al. Dust in ITER: Diagnostics and removal techniques. Journal of Nuclear Materials. 2009;**386-388**:882-883. DOI: 10.1016/j.jnucmat.2008.12.195

[9] Malizia A, Poggi LA, Ciparisse J-F, Rossi R, Bellecci C, Gaudi P. A review of dangerous dust in fusion reactors: From its creation to its resuspension in case of LOCA and LOVA. Energies. 2016;**9**(8):578. DOI: 10.3390/en9080578

[10] Baron-Wiechec A, Fortuna-Zaleśna E, Grzonka J, Rubel M, Widdowson A, Ayres C, et al. First dust study in JET with the ITER-like wall: Sampling, analysis and classification. Nuclear Fusion. 2015;**55**(11):113033 (7 pp). DOI: 10.1088/0029-5515/55/11/113033

[11] Ratynskaia S, Tolias P, De Angeli M, Weinzettl V, Matejicek J, Bykov I, et al. Tungsten dust remobilization under steady-state and transient plasma conditions. Nuclear Materials and Energy. 2017;**12**:569-574. DOI: 10.1016/j.nme.2016.10.021

[12] Wang H, Fang ZZ, Hwang KS, Zhang H, Siddle D. Sinter-ability of nanocrystalline tungsten powder. International Journal of Refractory Metals & Hard Materials. 2010;**28**:312-316. DOI: 10.1016/j.ijrmhm.2009.11.003

[13] Syed MA, Manzoor U, Shah I, Bukhari SH. Antibacterial effects of tungsten nanoparticles on the Escherichia coli strains isolated from catheterized urinary tract infection (UTI) cases and Staphylococcus aureus. New Microbiologica. 2010;**33**:329-335. Available from: http://www.newmicrobiologica.org/PUB/allegati_pdf/2010/4/329.pdf

[14] Lita AE, Rosenberg D, Nam S, Miller AJ, Balzar D, Kaatz LM, et al. Tuning of tungsten thin film superconducting transition temperature for fabrication of photon number resolving detectors. IEEE Transactions on Applied Superconductivity. 2005;**15**:3528-3531. DOI: 10.1109/TASC.2005.849033

[15] Pai CF, Liu L, Li Y, Tseng HW, Ralph DC, Buhrman RA. Spin transfer torque devices utilizing the giant spin Hall effect of tungsten. Applied Physics Letters. 2012;**101**(12):122404. DOI: 10.1063/1.4753947

[16] Long HW, Zeng W, Zhang H. Synthesis of WO_3 and its gas sensing: A review. Journal of Materials Science Materials in Electronics. 2015;**26**(7):4698-4707. DOI: 10.1007/s10854-015-2896-4

[17] Adhikari S, Chandra KS, Kim DH, Madras G, Sarkar D. Understanding the morphological effects of WO_3 photocatalysts for the degradation of organic pollutants. Advanced Powder Technology. 2018;**29**(7):1591-1600. DOI: 10.1016/j.apt.2018.03.024

[18] Zhao Y. WO_3 for photoelectro-chemical water splitting: from plain films to 3D architectures [thesis]. Eindhoven: Technische Universiteit Eindhoven; 2019. p. 135

[19] Schottle C, Bockstaller P, Gerthsenb D, Feldmann C. Tungsten nanoparticles from liquid-ammonia-based synthesis. Chemical Communications. 2014;**50**(35):4547-4550. DOI: 10.1039/c3cc49854a

[20] Sahoo PK, Kamal SSK, Premkumar M, Kumar TJ, Sreedhar B, Singh AK, et al. Synthesis of tungsten nanoparticles by solvothermal decomposition of tungsten hexacarbonyl. International Journal of Refractory Metals & Hard Materials. 2009;**27**:784-791. DOI: 10.1016/j.ijrmhm.2009.01.005

[21] Oda E, Ameyama K, Yamaguchi S. Fabrication of nano grain tungsten compact by mechanical milling process and its high temperature properties. Materials Science Forum. 2006;**503-504**: 573-578. DOI: 10.4028/www.scientific.net/MSF.503-504.573

[22] Antony LVM, O'Dell JS, McKechnie TN, Power C, Hemker K, Mendis B. US pioneers 'high speed' tiny tungsten. Metal Powder Report. 2006;**61**(11):16-19. DOI: 10.1016/S0026-0657(06)70761-5

[23] Sarathi R, Sindhu TK, Chakravarthy SR, Sharma A, Nagesh KV. Generation and characterization of nano-tungsten particles formed by wire explosion process. Journal of Alloys and Compounds. 2009;**475**(1-2):658-663. DOI: 10.1016/j.jallcom.2008.07.092

[24] Xiao J, Liu P, Liang Y, Li HB, Yang GW. Super-stable ultrafine beta-tungsten nanocrystals with metastable phase and related magnetism. Nanoscale. 2013;**5**(3):899-903. DOI: 10.1039/c2nr33484d

[25] Stokker-Cheregi F, Acsente T, Enculescu I, Grisolia C, Dinescu G. Tungsten and aluminium nanoparticles synthesized by laser ablation in liquids. Digest Journal of Nanomaterials and Biostructures. 2012;**7**(4):1569-1576. Available from: http://www.chalcogen.ro/1569_Stokker.pdf

[26] Samsonov D, Goree J. Particle growth in a sputtering discharge. Journal of Vacuum Science & Technology A. 1999;**17**:2835. DOI: 10.1116/1.581951

[27] Kumar KK, Couedel L, Arnas C. Growth of tungsten nanoparticles in direct-current argon glow discharges. Physics of Plasmas. 2013;**20**:043707. DOI: 10.1063/1.4802809

[28] Acsente T, Negrea RF, Nistor LC, Logofatu C, Matei E, Birjega R, et al. Synthesis of flower-like tungsten nanoparticles by magnetron sputtering combined with gas aggregation. European Physical Journal. 2015;**69**(6):161. DOI: 10.1140/epjd/e2015-60097-4

[29] Acsente T, Negrea RF, Nistor LC, Matei E, Grisolia C, Birjega R, et al. Tungsten nanoparticles with controlled shape and crystallinity obtained by magnetron sputtering and gas aggregation. Materials Letters. 2017;**200**:121-124. DOI: 10.1016/j.matlet.2017.04.105

[30] Haberland H, Karrais M, Mall M, Turner Y. Thin films from energetic cluster impact: A feasibility study. Journal of Vacuum Science & Technology A. 1992;**10**:3266. DOI: 10.1116/1.577853

[31] Smirnov BM, Shyjumon I, Hippler R. Flow of nanosize cluster-containing plasma in a magnetron discharge. Physical Review E. 2007;**75**(6):066402. DOI: 10.1103/PhysRevE.75.066402

[32] Huttel Y. Gas-Phase Synthesis of Nanoparticles. 1st ed. Weinheim: Wiley-VCH; 2017. p. 402. DOI: 10.1002/9783527698417

[33] Haberland H, Karrais M, Mall M. A new type of cluster and cluster ion-source. Zeitschrift Fur Physik D-Atoms Molecules and Clusters. 1991;**20**:413-415. DOI: 10.1007/BF01544025

[34] Majumdar A, Ganeva M, Kopp D, Datta D, Mishra P, Bhattacharayya S, et al. Surface morphology and composition of films grown by size-selected Cu nanoclusters. Vacuum. 2008;**83**(4):719-723. DOI: 10.1016/j.vacuum.2008.05.022

[35] Polonskyi O, Kylian O, Solar P, Artemenko A, Kousal J, Slavınska D, et al. Nylon-sputtered nanoparticles: Fabrication and basic properties. Journal of Physics D-Applied Physics. 2012;**45**(49):495301. DOI: 10.1088/0022-3727/45/49/495301

[36] Krishnan G, Negrea RF, Ghica C, ten Brink GH, Kooi BJ, Palasantzas G. Synthesis and exceptional thermal stability of Mg-based bimetallic nanoparticles during hydrogenation. Nanoscale. 2014;**6**:11963-11970. DOI: 10.1039/c4nr03885a

[37] Llamosa D, Ruano M, Martinez L, Mayoral A, Roman E, Garcia-Hernandez M, et al. The ultimate step towards a tailored engineering of core–shell and core–shell–shell nanoparticles. Nanoscale. 2014;**6**:13483. DOI: 10.1039/c4nr02913e

[38] Wegner K, Piseri P, Vahedi Tafreshi H, Milani P. Cluster beam deposition: A tool for nanoscale science and technology. Journal of Physics D-Applied Physics. 2006;**39**:R439-R459. DOI: 10.1088/0022-3727/39/22/R02

[39] Grisolia C, Hodille E, Chene J, Garcia-Argote S, Pieters G, El-Kharbachi A, et al. Tritium absorption and desorption in ITER relevant materials: Comparative study of tungsten dust and massive samples. Journal of Nuclear Materials. 2015;**463**:885-888. DOI: 10.1016/j.jnucmat.2014.10.089

[40] El-Kharbachi A, Chêne J, Garcia-Argote S, Marchetti L, Martin F, Miserque F, et al. Tritium absorption/desorption in ITER-like tungsten particles. International Journal of Hydrogen Energy. 2014;**39**(20):10525-10536. DOI: 10.1016/j.ijhydene.2014.05.023

[41] Bernard E, Jambon F, Georges I, Sanles Sobrido M, Rose J, Herlin-Boime N, et al. Design of model tokamak particles for future toxicity studies: Morphology and physical characterization. Fusion Engineering and Design. 2019;**145**:60-65. DOI: 10.1016/j.fusengdes.2019.05.037

[42] George I, Uboldi C, Bernard E, et al. Toxicological assessment of ITER-like

tungsten nanoparticles using an In vitro 3D human airway epithelium model. Nanomaterials (Basel). 2019;**9**(10):1374. DOI: 10.3390/nano9101374

[43] Uboldi C, Sanles Sobrido M, Bernard E, Tassistro V, Herlin-Boime N, Vrel D, et al. In vitro analysis of the effects of ITER-like tungsten nanoparticles: Cytotoxicity and epigenotoxicity in BEAS-2B cells. Nanomaterials (Basel). 2019;**9**(9):1233. DOI: 10.3390/nano9091233

[44] Shi F. Introductory Chapter: Basic Theory of Magnetron Sputtering [Online First]. Rijeka: IntechOpen; 2018. DOI: 10.5772/intechopen.80550. Available from: https://www.intechopen.com/online-first/introductory-chapter-basic-theory-of-magnetron-sputtering

[45] Kelly PJ, Arnell RD. Magnetron sputtering: A review of recent developments and applications. Vacuum. 2000;**56**(3):159-172. DOI: 10.1016/S0042-207X(99)00189-X

[46] Smirnov BM. Nanoclusters and Microparticles in Gases and Vapors. Berlin: De Gruyter; 2012. p. 264. DOI: 10.1515/9783110273991

[47] Ganeva M. Formation of metal nano-size clusters with a DC magnetron-based gas aggregation source [thesis]. Greifswald: Mathematisch-Naturwissenschaftliche Fakultät/Institut für Physik; 2013

[48] Peter T, Polonskyi O, Gojdka B, Ahadi AM, Strunskus T, Zaporojtchenko V, et al. Influence of reactive gas admixture on transition metal cluster nucleation in a gas aggregation cluster source. Journal of Applied Physics. 2012;**112**:114321. DOI: 10.1063/1.4768528

[49] Marek A, Valter J, Kadlec S, Vyskocil J. Gas aggregation nanocluster source-reactive sputter deposition of copper and titanium nanoclusters. Surface and Coating Technology. 2011;**205**(S2):S573-S576. DOI: 10.1016/j.surfcoat.2010.12.027

[50] Vollath D. Plasma synthesis of nanopowders. Journal of Nanoparticle Research. 2008;**10**:39-57. DOI: 10.1007/s11051-008-9427-7

[51] Kimoto K, Nishida I. The crystal habits of small particles of aluminium and silver prepared by evaporation in clean atmosphere of argon. Japanese Journal of Applied Physics. 1977;**16**(6):941-948. DOI: 10.1143/JJAP.16.941

[52] Arnas C, Chami A, Couedel L, Acsente T, Cabie M, Neisius T. Thermal balance of tungsten monocrystalline nanoparticles in high pressure magnetron discharges. Physics of Plasmas. 2019;**26**:053706. DOI: 10.1063/1.5095932

[53] EL KA, Chene J, Garcia-Argote S, Marchetti L, Martin F, Miserque F, et al. Tritium absortion/desorption in ITER-like tungsten particles. International Journal of Hydrogen Energy. 2014;**39**(20):10525-10536. DOI: 10.1016/j.ijhydene.2014.05.023

[54] Grisolia C, Gensdarmes F, Peillon S, Dougniaux G, Bernard E, Autricque A, et al. Current investigations on tritiated dust and its impact on tokamak safety. Nuclear Fusion. 2019;**59**:086061. DOI: 10.1088/1741-4326/ab1a76

[55] Constant S, Huang J, Derouette JP, Wisniewski L. MucilAir: A novel in vitrohuman 3D airway epithelium model for assessing the potential hazard of nanoparticles and chemical compounds. Toxicology Letters. 2008;**180S**:S32-S246. DOI: 10.1016/j.toxlet.2008.06.042

[56] Carpen LG, Acsente T, Acasandrei MA, Matei E, Chilom CG, Savu DI, et al. The Interaction of Tungsten Dust with Human Skin Cells [Online First]. Rijeka: IntechOpen; 2019. DOI: 10.5772/intechopen.86632. Available from: https://www.intechopen.com/online-first/the-interaction-of-tungsten-dust-with-human-skin-cells